Available online at www.sciencedirect.com

ScienceDirect

journal homepage: www.elsevier.com/locate/he

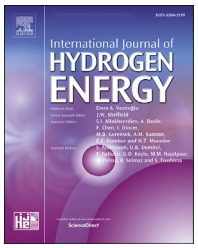

Anomalous blow-off limit of methane-air premixed flame in a micro preheated combustor with a flame holder

Jianlong Wan[*], *Haibo Zhao*[**]

State Key Laboratory of Coal Combustion, School of Energy and Power Engineering, Huazhong University of Science and Technology, Wuhan 430074, PR China

HIGHLIGHTS

- Regime diagram of flame behavior for different operating conditions is obtained.
- There are difference in the blow-off limit between the micro and mesoscale burners.
- The anomalous blow-off phenomenon is first found in the micro combustors.
- The underlying mechanisms of the anomalous blow-off are systematically revealed.
- The intrinsic unification of the anomalous and normal blow-off is discussed.

ARTICLE INFO

Article history:
Received 11 May 2020
Received in revised form
11 August 2020
Accepted 15 August 2020
Available online 28 September 2020

Keywords:
Micro combustion
Flame holder
Heat recirculation
Premixed flame
Blow-off

ABSTRACT

The present work first reports the combustion characteristics of methane/air premixed fuel mixture (Lewis number $Le \approx 1.0$) at different Reynolds numbers (Re) in a micro preheated combustor with a flame holder which can be used as heat source for the micro power generators. Unexpectedly, the previously reported anomalous blow-off of lean H_2/CH_4/air ($Le < 1.0$) premixed flame in the mesoscale combustor appears in the present micro combustor, which is observed for the first time. The flame dynamics in the micro combustor also presents other new features comparing with that in the similar mesoscale combustor. Three neighboring cases ($Re = 40$, 80, and 120) are adopted to reveal the underlying mechanisms of the anomalous blow-off in terms of the flow field, stretch effect, conjugate heat exchange, and preferential transport effect. A better heat recirculation effect results in the increase of blow-off limit from $Re = 120$ to 80. A worse flow recirculation effect, a larger heat loss ratio to the environment, and a worse preferential transport effect lead to the decrease of blow-off limit from $Re = 80$ to 40. In the end, the critical standoff distance between the flame root and flame holder presents a second-order function relation with the change of Re.

* *Corresponding author.*
** *Corresponding author.*
E-mail addresses: jlw@hust.edu.cn (J. Wan), hzhao@mail.hust.edu.cn (H. Zhao).
https://doi.org/10.1016/j.ijhydene.2020.08.130

Introduction

Because of the energy densities of hydrocarbon fuels are much higher than that of conventional electrochemical batteries, combustion-based miniature power generators have attracted extensive attention, which can provide power sources for micro-electro-mechanic systems (MEMS) [1]. However, the large surface area-to-volume ratio of the micro combustor leads to the sharp increase of the heat loss to the environment and the occurrence of the flame quenching near the inner wall of the combustor [2]. Also, the residence time of gaseous mixture is too short in the micro combustion chamber [3]. As a result, the flame stabilization sharply decreases and many unstable flame behaviors appear in the micro burners, such as the oscillating flames [4,5] and the x-shaped spinning flames [6,7]. Therefore, the significant improvement of the flame stabilization in the micro combustor is crucial for the development of the miniature power-generation devices.

To this end, many strategies were developed to improve micro flame stabilization. For example, the heat recirculation method was frequently adopted to stabilize the flames in the small burners owing to compensate for the heat loss to the environment. Kuo & Ronney [8] employed a special "Swiss-roll" burner to broaden the flammability limits of premixed flames. Tang et al. [9] found that the heat recirculation can obviously improve the thermal performance of the micro plate combustor. The operating range of the stable flame in the micro combustors with porous media also can be effectively broadened owing to the heat recirculation [9–11]. Besides, Jiang et al. [12] found that the flame stability can be well improved in a small combustor with porous wall which can significantly preheat the fresh mixture. However, the heat recirculation method cannot well anchor the flame although it can obviously broaden the flammability limit of fuel mixture in the micro combustor, which leads to a narrow blowout limits in these combustors.

The flow recirculation method can effectively anchor the micro flame via structural design, such as the bluff-body [13] and cavity [14–16]. Yang et al. [17] observed that the hydrogen/air premixed flame can be well anchored by the recirculation zone behind the backward-facing step in a micro-tube combustor. The wall temperature magnitude of the micro tube-combustor can also be increased by the backward-facing step [18]. Wan et al. [19–22] found that the anchoring performance of premixed flame is significantly improved by the recirculation zone within the wall cavities in a micro or mesoscale combustor. Wang et al. [23] observed that the hydrogen jet combuston stability is remarkably enhanced by the combined cavity shear-layer/recirculation. Additionally, Wan et al. [24,25] and Li et al. [26] pointed out that the blowout limit of premixed flame can be significantly broadened in a micro or mesoscale combustor with bluff-body. Pan et al. [27] observed that the bluff-body ball can prevent the downstream movement of the flame in a micro plate combustor. Additionally, the inserted bluff-body can further improve the thermal performance of the micro combustor [28]. It should be pointed out that although the flow recirculation method can remarkably anchor the flame and broaden the flame blowout limit, the flammability limits based on the equivalence ratio in these combustors with special cconfigurations are not wide.

Therefore, it is expected that the flame blowout limit and the flammability limits can be both broadened if the advantages of heat and flow recirculation can be synergistically utilized. To this end, a novel micro preheated combustor with a flame holder was developed in our previous publications [29–32]. And results indeed demonstrated that both the blowout limits and flammability limits of methane/air premixed mixture were large in this combustor [29–31]. Recently, a non-monotonic blow-off limnits were found in this combustor at various blockage ratios [33]. In order to provide the guideline for applying the present combustor as heat source for the micro power generators, the present study detailedly reports the distribution characteristics of flame behavior at fuel lean condition, and the anomalous blow-off phenomenon was observed. The present work can help researchers to gain insight into the micro flame dynamics under the synergistic effect of heat and flow recirculation.

Numerical methods

Geometric model

Fig. 1 schematically shows the geometric structure of the preheated combustor with a flame holder. It can be seen that the combustor is a two-dimensional symmetrical structure. The whole flow channel is divided into the preheating channels and combustion chamber by the yellow solid lines. The wall thickness (δ) is 0.5 mm. The width and length of the flame holder are 1.0 mm and 6.0 mm, respectively. The widths of preheating channel and combustion chamber are 0.5 mm and 2.0 mm, respectively. The other geometrical sizes of the combustor are shown in Fig. 1.

Computation scheme

In the present work, the fuel and oxidizer are methane and air, respectively. When the inlet velocity of the cold fuel mixture V_{in} is 10 m/s, the corresponding Reynolds number Re is 400, and the laminar unsteady state model is adopted in the computation [30,34]. The detailed explanation about the governing equations can be obtained from our previous publication [35]. Under a constant Re, the equivalence ratio (φ) of fuel mixture decreases from $\varphi = 1.0$ with an interval of 0.025 until flame blows off. Same with the previous publication [30,35], the stainless steel, whose thermal conductivity is 24 W/(m·K), is adopted to manufacture the present combustor [36]. The combustion reaction of methane/air is simulated using the detailed C1 mechanism (18 species and 58 reactions) [37], and the CHEMKIN databases [38] is employed to provide the thermodynamic and transport properties of the reaction species. The mixture-averaged formulation is adopted to compute the species transport properties. The Soret diffusion effect is ignored here due to the Soret diffusion effect is generally much smaller than Fickian diffusion effect for methane-air mixture with the Lewis number $Le = 1.0$ [39]. The heat conduction in the solid walls and fluid are computed by

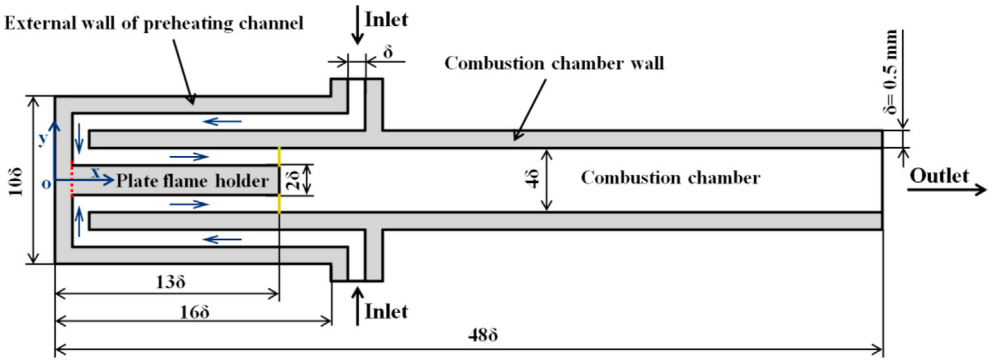

Fig. 1 – Schematic of the micro preheated combustor with a flame holder.

Table 1 – Boundary conditions for numerical simulation.

Position	Settings
Inner wall	Chemically inert with no-slip
Inlet	Uniform concentration and velocity distributions at 300 K
Outlet	Neumann boundary
Interface between the fluid and solid	The method of "Coupled"

the Fourier's law. The heat loss from the outer wall of the combustor to the environment includes the natural convection and heat radiation [34]. Table 1 shows the boundary conditions for numerical simulation:

The ANSYS Fluent [40] is employed to solve the mass, momentum, energy, and species conservation equations. Same as before, in order to reasonably reduce the computation load, half of the configuration was employed [29,30]. Grid independency is checked, and results show that the grid size of 50 μm is sufficiently fine to capture the flame structure [29,30]. Further refinement of the meshes (the minimum grid size is 25 μm) near the flame holder is adopted [29,30]. In the present unsteady-state simulation, a time step of 1.0×10^{-6} s is employed [34,35]. The convergence criteria for the residuals of the computational results are smaller than 1.0×10^{-6}. It should be pointed out that the present numerical models and methods were also employed to simulate the combustion characteristics of methane/air premixed mixture in a similar mesoscale combustor in our previous studies, and the computational results is agreement with the experimental data [31,41,42]. Thus, the numerical models and methods adopted in this work are reasonable, and the current numerical results are solid.

Results and discussions

Regime diagram of flame behavior

Fig. 2 displays the regime diagram of methane/air flame dynamics at different Reynolds numbers and equivalence ratios at lean fuel. It can be seen there are four kinds of flame behaviors, i.e., the stable flame, pulsating flame, the flame with repetitive flashback and pulsating (FRFP), and flame blow-off, which have been detailedly described in our previous publication [35]. At $Re \geq 160$, the flame is periodically pulsating over time until blow-off. At $Re \leq 120$, the stable flame appears near the blow-off limit. Particularly, the FRFP only occurs at the cases around the stoichiometric ratio for $Re = 80$. Preliminary analysis indicates that: when $Re > 80$, the flow velocity in the preheating channel is too fast for the flashback; when $Re < 80$, the heat loss ratio from the combustor to environment is too large for the flashback due to the small input fuel quantity, which will be confirmed in the following section. The FRFP occurs at $Re = 80$ owing to a good combustion condition (the suitable flow velocity and fuel quantity). More importantly, it is unexpected that the flame blow-off limit decreases at first and then increase with the decrease of Re, and the lowest blow-off limit appears at $Re = 80$. The phenomenon which the blow-off limit increases with a decreasing Re is the so-called "anomalous blow-off" [43,44]. Accordingly, the stage in

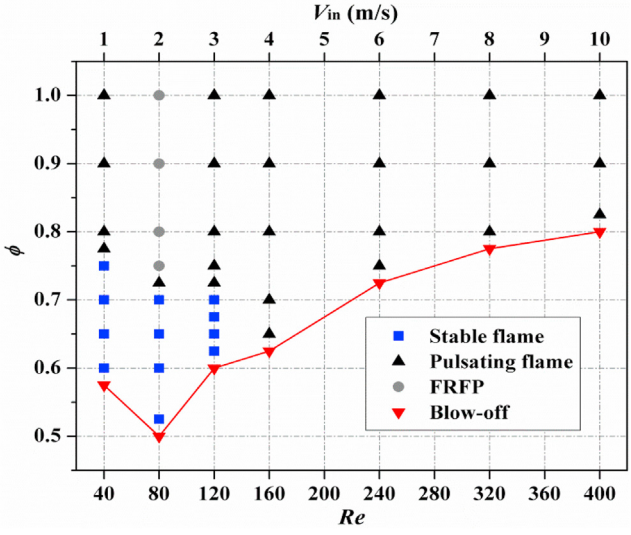

Fig. 2 – Regime diagram of flame behavior for different Re and φ in the present combustor.

which the blow-off limit decreases with a decreasing *Re* is called "normal blow-off". Shoshin et al. [43] and Jiménez et al. [44] found the anomalous blow-off phenomenon in a mesoscale combustor with the bluff body integrated using the lean fuel mixture of H_2/CH_4/air (the Lewis number $Le < 1.0$) as the fuel via direct numerical simulation. The anomalous blow-off phenomenon was caused by the preferential diffusion effect. Recently, the anomalous blow-off of methane/air ($Le \approx 1.0$) premixed flame was experimentally observed at first by us in a mesoscale combustor with a plate flame holder and preheating channels [45]. However, the present differences of blow-off limit between different *Re* are significantly larger than that in the similar mesoscale combustor, which is a new feature of flame dynamics in the micro combustor. Three neighboring cases ($Re = 40$, 80, and 120) are adopted to reveal the underlying mechanisms responsible for the present anomalous blow-off phenomenon in the following sections.

Mechanisms of anomalous blow-off

Same as before, the normalized 15% of maximum Y_{HCO} isoline is used to mark the flame front for the convenience of quantitative discussion. Moreover, as the laminar premixed flame stabilized on a bluff body is significantly influenced by the flow field, the stretch effect, the conjugate heat exchange, and the preferential transport effect [39], the underlying mechanisms of the anomalous blow-off will be discussed from the above four aspects.

Flow field

The flow field in the combustor with the flame holder mainly has two direct effects on the flame stabilization. On the one hand, the recirculation zone (*RZ*) generated behind the flame holder is beneficial for the flame stabilization (the positive effect). On the other hand, the incoming flow directly pushes the flame front out of the *RZ* downstream, which is detrimental for the flame stabilization (the negative effect). For the positive aspect, a larger counter flow in the recirculation zone, which can extend the residence time of gaseous mixture and provide a reactive radicals pool, can prevent the flame from being pushed downstream. Fig. 3 shows that the recirculation zone increases with the *Re*. And it was observed that the length of *RZ* (the distance between the most downstream location of *RZ* and the flame holder) at $Re = 40$, 80, and 120 are 0.05 mm, 0.49 mm, and 0.86 mm, respectively. It can be seen that the *RZ* at $Re = 40$ is very small, which nearly can be ignored. Moreover, the area of flame root within the *RZ* is also larger for a higher *Re*, which is beneficial for the flame root stabilization. Thus, the worse flow recirculation effect is one of the factors which decrease the blow-off limit from $Re = 80$ to 40.

For the negative effect aspect, Fig. 4 shows the acute angle between the local flow direction and positive direction of *x*-axis (θ_{flow}), the local flow velocity (V_{local}), the acute angle between the normal direction of the flame front and flow direction (θ_n), and the local flow velocity at the normal direction of the flame front (V_n) along with the upstream boundary of flame front for different *Re*. It can be seen that the $|\theta_{flow}|$ decreases with the increase of *Re*, which is mainly caused by the obvious increase of the y-component of flow velocity. The recirculation zone at $Re = 80$ and 120 makes the $|\theta_{flow}|$ slightly decreases at first and then increases along with the flame front towards downstream. Moreover, as expected, the local flow velocity is larger for a bigger *Re*. However, a larger V_{local} does not always mean a larger V_n which is also determined by the θ_n. Fig. 4b presents that the θ_n is almost the same near the middle of flame front ($\sim 0.4 \le l \le 0.8$) under one constant *Re*, and it remarkably increases with the increase of *Re*, which will decrease the component of the V_{local} at the normal direction of flame front because $V_n = V_{local} \times \cos\theta_n$. As a comprehensive result of V_{local} and θ_n, it is unexpected that the V_n at $Re = 80$ is the largest and that at $Re = 120$ is the smallest among of them. It is calculated that the average V_n at $Re = 40$, 80, and 120 are 1.73 m/s, 2.24 m/s, and 1.70 m/s, respectively. It is known that the $|S| = |V_n|$ (*S* is the flame speed) is the necessary condition for the stable flame. When $|V_n|$ is larger than $|S|$, the flame will be pushed downstream. Therefore, a larger V_n is detrimental for the flame stabilization. However, the result shows that the blow-off limit at $Re = 80$ is the largest, so it is argued that the negative effect of flow field is insignificant for the non-monotonic blow-off limit.

Stretch effect

It is known that the stretch effect has a negative effect on the flame stabilization out of the recirculation zone. Therefore, the stretch rate (k) along with the flame front is quantitatively calculated here, and $k = k_c + k_s$: k_c and k_s are the curvature and strain rates, respectively [39]. The curvature (k_c) and strain (k_s) can be calculated by the following equations [46]:

$$k_c = -(un_x + vn_y)\left(\frac{dn_x}{dx} + \frac{dn_y}{dy}\right) \tag{1}$$

$$k_s = -n_x n_y\left(\frac{\partial u}{\partial y} + \frac{\partial v}{\partial x}\right) - n_x^2\frac{\partial u}{\partial x} - n_y^2\frac{\partial v}{\partial y} \tag{2}$$

where n is the normal direction of the flame front; u and v are the x and y components of the flow velocity, respectively; $-n_x n_y\left(\frac{du}{dy} + \frac{dv}{dx}\right)$ is the contribution of shear ($k_{s,s}$); $-n_x^2\frac{\partial u}{\partial x} - n_y^2\frac{\partial v}{\partial y}$ is the contributions of normal strain ($k_{s,n}$).

Fig. 5 shows the k_c, k_s and k profiles along with the upstream boundary of flame front towards downstream for different *Re*. Fig. 5a indicates that $|k_c|$ is significantly smaller than $|k_s|$, so the contribution of the k_c to k can be neglected (*i.e.*, $k \approx k_s$), which is caused by a flat flame shape. Moreover, Fig. 5a shows that the k_s at $Re = 40$ is smaller and that at $Re = 80$ and 120 are larger. Further, near the middle of the flame front ($\sim 0.25 \le l \le 0.9$), the $|k_s|$ at $Re = 80$ is larger than that at $Re = 120$. It is calculated from Fig. 5b that the average $|k|$ at $Re = 40$, 80, and 120 are 3083.6 1/s, 4025.1 1/s, and 3254.7 1/s, respectively, which means that the stretch effect increases firstly and then decreases with the increase of *Re*. In other words, the stretch effect at $Re = 80$ is the largest among of them, which is consistence with the change rule of V_n. However, this opposite with the change trend of blow-off limit. Therefore, the stretch effect is insignificant for the non-monotonic blow-off limit.

Conjugate heat exchange

It is know that the flame stabilization is significantly influenced by the heat exchange effect of the solid walls. On the one hand, the heat loss from the flame to the solid walls is

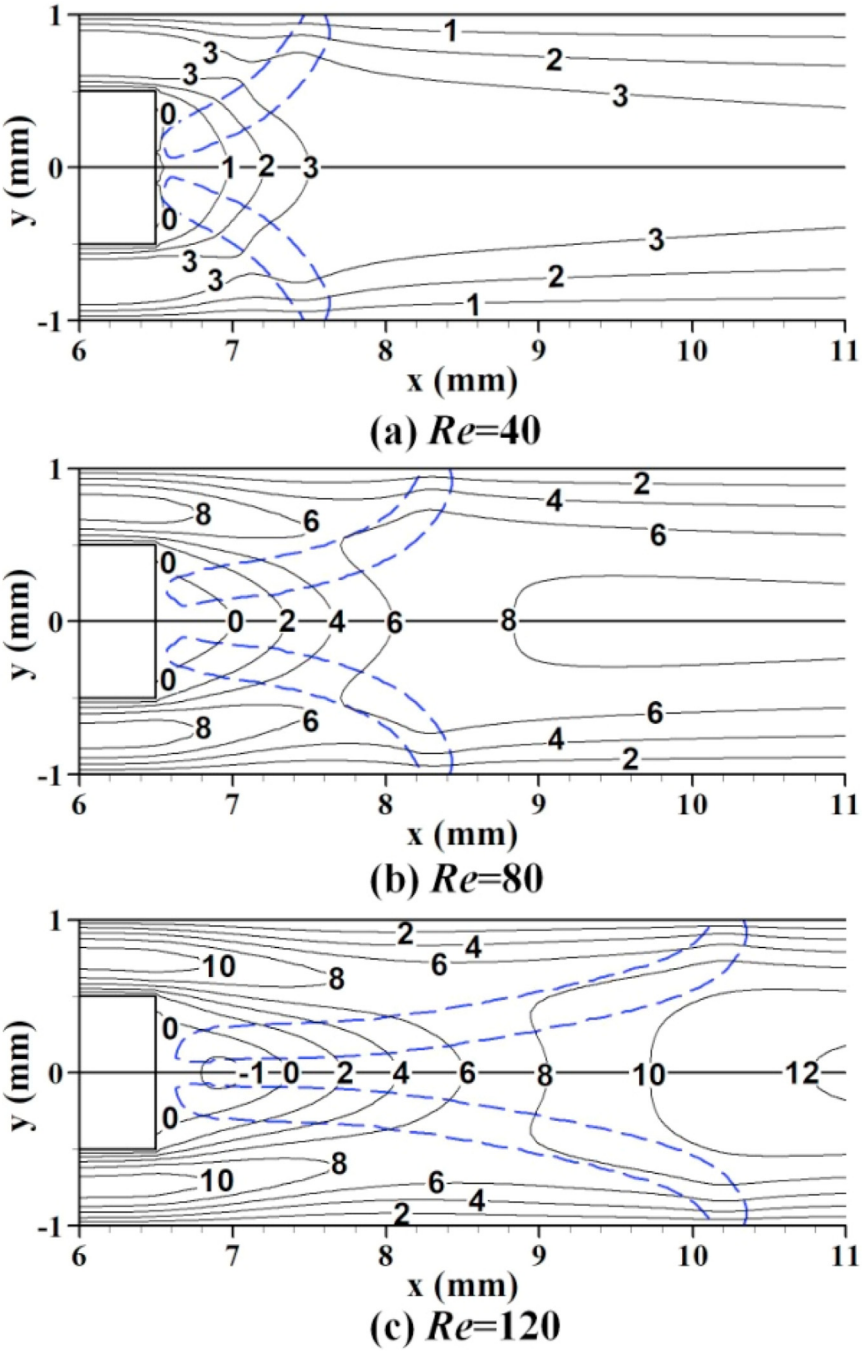

Fig. 3 – Flow field with overlaid flame front (blue dash line) for different *Re* at $\varphi = 0.65$. (For interpretation of the references to color in this figure legend, the reader is referred to the Web version of this article.)

detrimental for the flame stabilization (the negative effect). On the other hand, the heat recirculation effect of solid walls which can significantly improve the fresh mixture temperature is beneficial for the flame stabilization (the positive effect). In order to evaluate the heat loss from the flame root to holder, Fig. 6 presents the heat flux entering the end wall of flame holder (the negative value means the heat loss from the flame root to holder). It can be seen that the amount of heat loss increases firstly and then decreases with the decrease of *Re*. It is calculated that the average heat flux at $Re = 120$, 80, and 40 are −166,801 W/m^2, -191,682 W/m^2 and -176,971 W/m^2, respectively. This is a comprehensive result of the flame root temperature and the distance between the flame root and flame holder. Concretely, a higher temperature of flame root and a shorter distance between the flame root and flame holder result in the largest heat loss from the flame root to the flame holder at $Re = 80$, which is opposite with the change trend of blow-off limit. Therefore, the heat loss from the flame root to the flame holder is insignificant for determining the blow-off limit.

Moreover, the total heat loss from the outer wall of the combustor to the environment is also calculated, as shown in

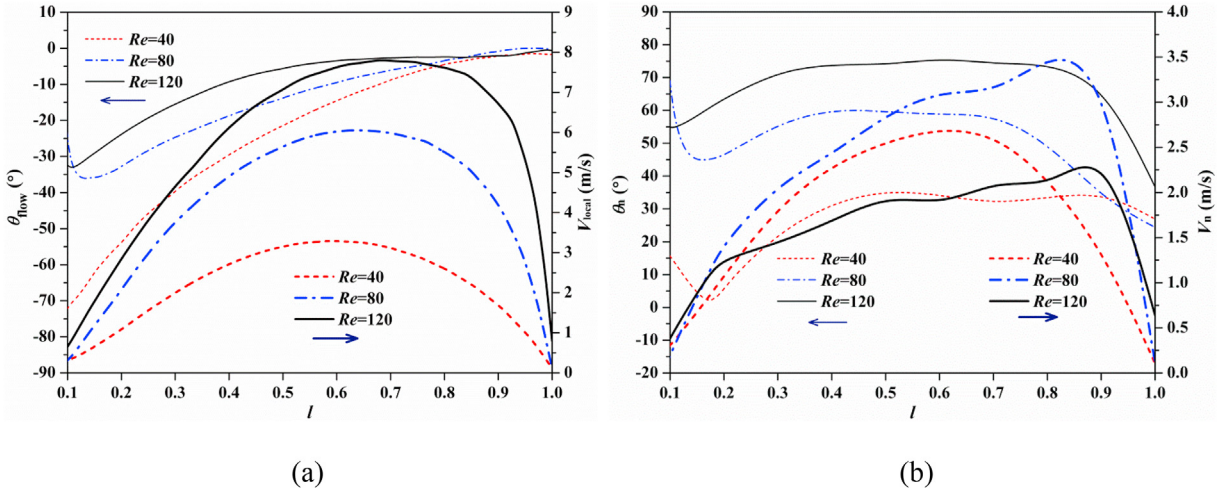

Fig. 4 – The profiles of the θ_{flow}, V_{local}, θ_n, and V_{local} out of the recirculation zone along with the upstream boundary of flame front (*i.e.*, the upstream boundary of 15% maximum Y_{HCO} isoline) for different *Re* at $\varphi = 0.65$. *L* is the dimensionless curved length of flame front. $L = l_f/l_t$: l_f is the curved distance between the anchoring location of the flame root (the point at the flame root which has the shortest distance to the flame holder) and any point at the upstream boundary of flame front; l_t is the total curved length of flame front).

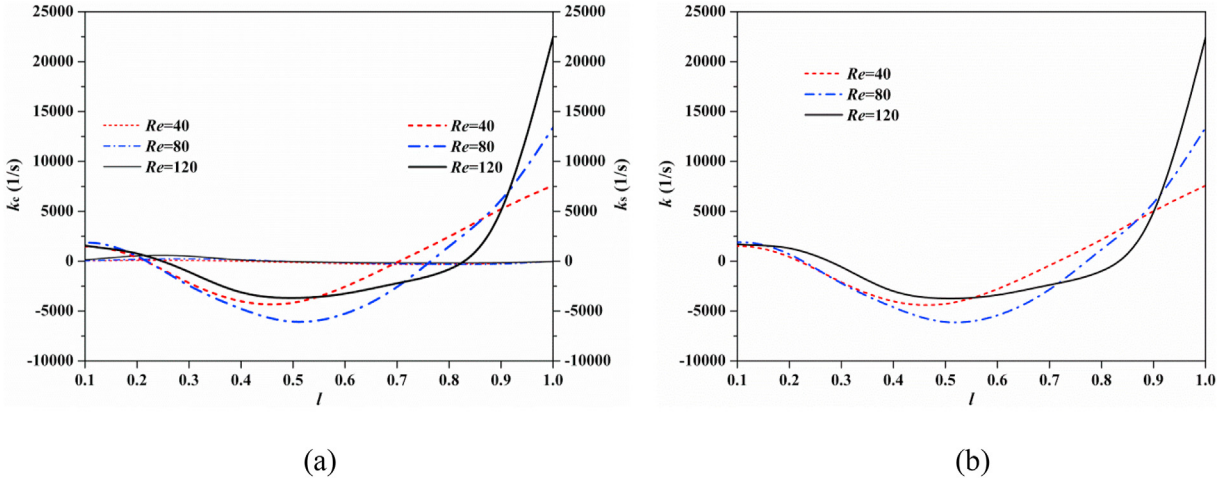

Fig. 5 – The k_c and k_s (a), and *k* (b) profiles along with the upstream boundary of flame front towards downstream for different *Re* at $\varphi = 0.65$.

Fig. 7. It can be seen that the absolute value of heat loss increases at first and then decreases with the decrease of *Re*. However, the heat loss ratio (the ratio between the absolute value of heat loss and the input caloric value involved in the fuel mixture) significantly increases with the decrease of *Re* mainly owing to the obvious decrease of fuel quantity, which presents a well linear relation. As we know, a larger total heat loss ratio from the combustor to the environment is detrimental for the flame stabilization, which is one of the factors which decrease the blow-off limit from *Re* = 80 to 40.

Furthermore, the fresh fuel mixture can be well preheated by the hear recirculation effect of the solid wall. It is calculated from Fig. 8a that the average gas temperature at the inlet of combustion chamber for *Re* = 40, 80, and 120 are 952.0 K, 936.8 K, and 760.0 K, respectively, *i.e.*, the preheated temperature of fresh fuel mixture decreases with the increase of *Re*. This is mainly because that the flame front remarkably shifts upstream with a decreasing *Re*. As a result, the horizontal wall temperature of flame holder and the inner wall temperature of combustion chamber wall in the preheating channel are higher for a smaller *Re*, as shown in Fig. 8b. It is calculated that the average horizontal wall temperatures of flame holder at *Re* = 40, 80, and 120 are 913.0, 891.2, and 705.2 K, respectively; the average inner surface temperatures of combustion chamber wall in the preheating channel at *Re* = 40, 80, and 120 are 940.6, 934.2, and 779.6 K, respectively. Also, the residence time of fuel mixture in the preheating channels is longer for a smaller *Re*. In one word, the heat recirculation effect on the fresh fuel mixture increases with the decrease of *Re*. A better heat recirculation effect is beneficial for the flame stabilization, which results in the increase of blow-off limit from *Re* = 120 to 80.

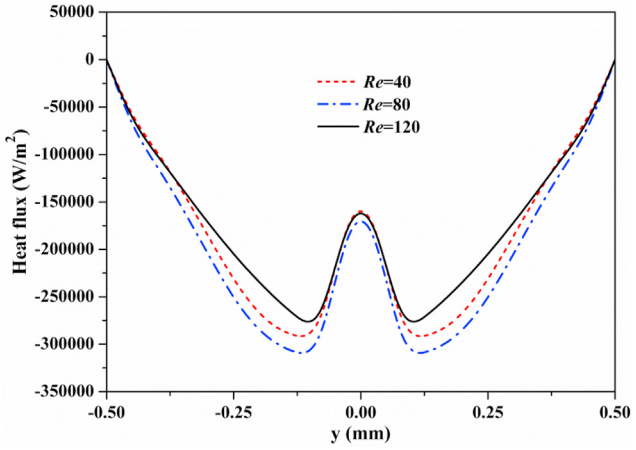

Fig. 6 – The heat flux profiles entering the end wall of the flame holder for different *Re* at $\varphi = 0.65$.

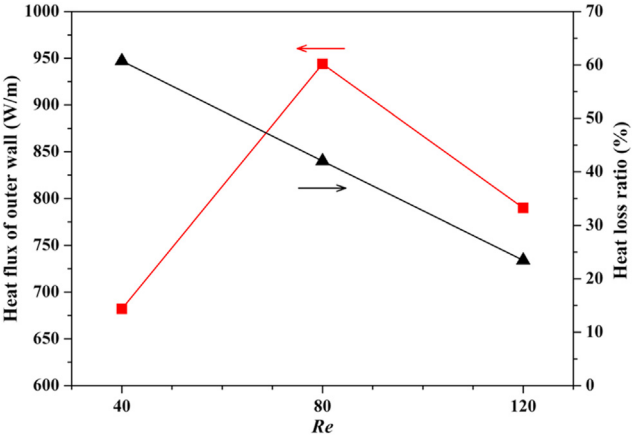

Fig. 7 – The total heat flux and heat loss ratio from the outer wall of combustor to the environment for different *Re* at $\varphi = 0.65$.

Preferential transport effect

Generally, the preferential transport effect, which is caused by the difference in mass diffusivities of the species, remarkably influences the local equivalence ratio (φ_{local}) [47,48]. This effect is different from the non-unity *Le* effect (the ratio between the thermal and mass diffusivities). The recirculation zone generated behind the bluff-body can improve the preferential transport effect owing to the enhanced flow two-dimensionality effect [47]. As the preferential transport effect can provide a locally high equivalence ratio zone near the flame root, which is beneficial for the flame stabilization. Barlow et al. [47] defined the φ_{local} based on the fuel/oxygen atom balance to quantitatively evaluate this effect, as presented in Eq. (3):

$$\varphi_{local} = \frac{0.5(X_{H_2} + X_{H_2O}) + X_{CO_2} + X_{CO} + 2X_{CH_4}}{0.5(X_{CO} + X_{H_2O}) + X_{O_2} + X_{CO_2}} \quad (3)$$

where X_i is the mole fraction of species *i*.

Fig. 9 shows the distribution characteristics of local equivalence ratio near the flame front, which indicates that the area of high φ_{local} just behind the flame holder tends to increase firstly and then decreases with the increase of *Re*. However, as the flame root at $Re = 120$ is closer to the center of the combustion chamber, the area of the flame root within the high φ_{local} (*i.e.*, the effecting area of high φ_{local} on the flame root) at $Re = 120$ is larger than that at $Re = 80$. To quantitatively characterize the distribution of φ_{local} near the flame root, Fig. 10 shows the φ_{local}-φ (departure from the incoming mixture equivalence ratio) profiles along with the upstream boundary of flame front for different *Re*. We can see that the φ_{local} at the flame root increases with the *Re*, and the φ_{local} at the anchoring location of flame root for $Re = 40$, 80, and 120 are 0.652, 0.663, and 0.676, respectively. The worse preferential transport effect (smaller φ_{local}) is detrimental for the flame stabilization, which is one of the factors which decrease the blow-off limit from $Re = 80$ to 40.

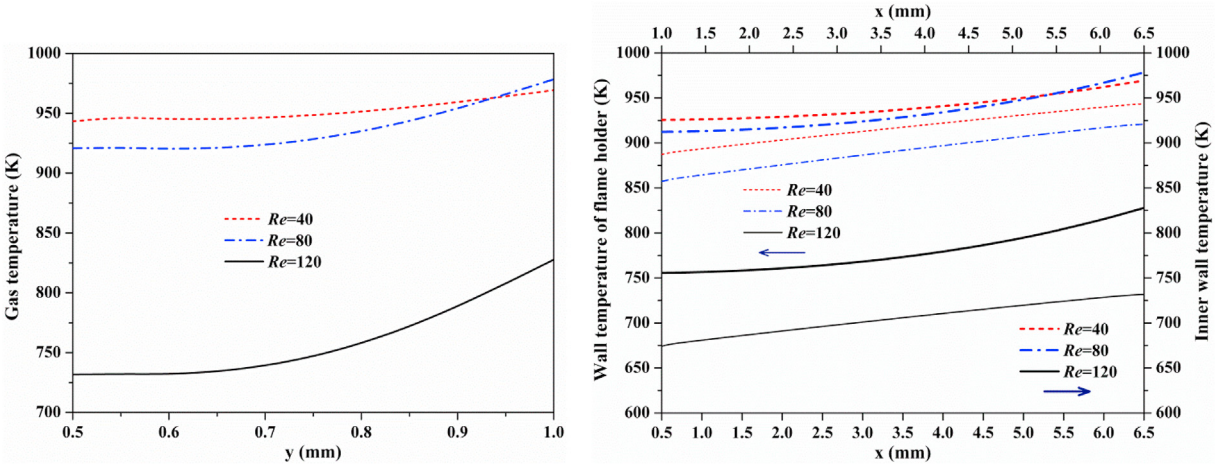

Fig. 8 – Gas temperature profiles at the inlet of combustion chamber ($x = 6.5$ mm, 0.5 mm $\le y \le$ 1.0 mm) (a); the temperature profiles of horizontal wall of flame holder ($y = 0.5$ mm, 0.5 mm $\le x \le$ 6.5 mm) and inner surface of combustion chamber wall ($y = 1.0$ mm, 1.0 mm $\le x \le$ 6.5 mm) (b) for different *Re* at $\varphi = 0.65$.

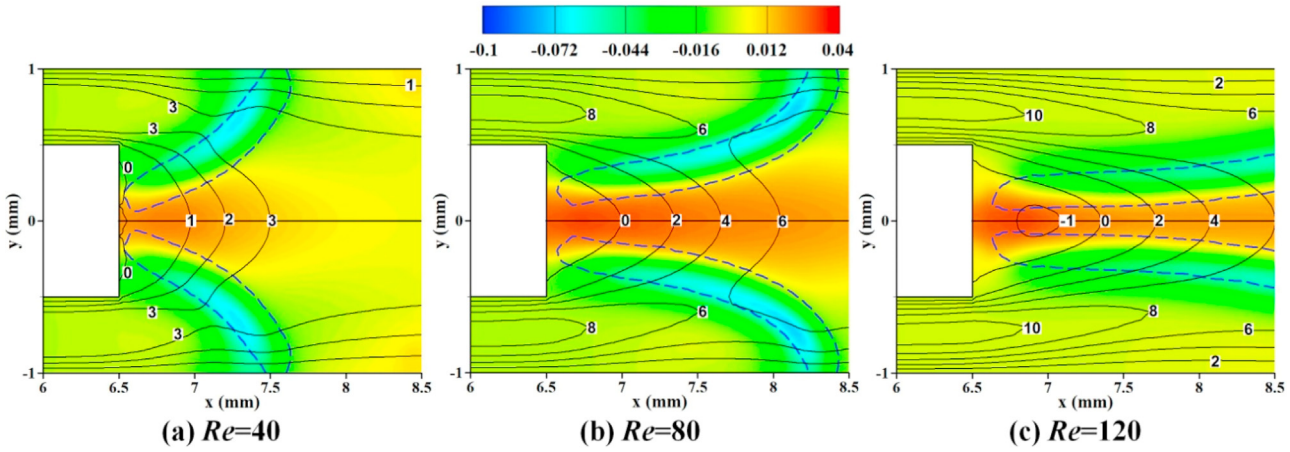

Fig. 9 – Colored contours of φ_{local} - φ_{in} and flow field with overlaid the flame front (bold dashed lines) for different *Re* at $\varphi = 0.65$.

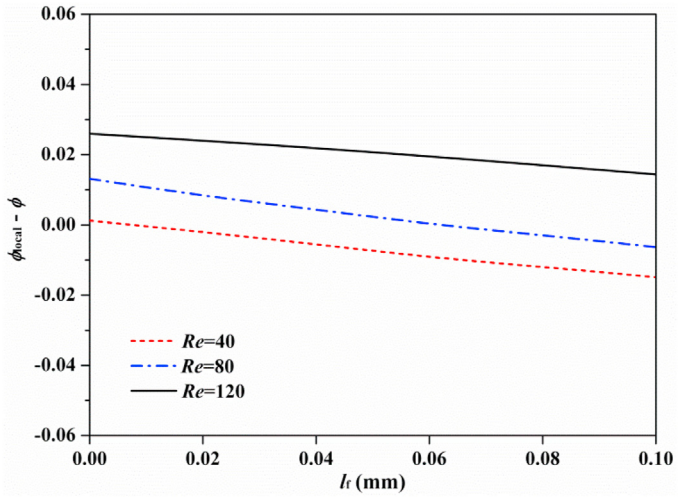

Fig. 10 – φ_{local}-φ profiles along with the upstream boundary of the flame front from the anchoring location of flame root ($l_f = 0.0$ mm) towards downstream for different *Re* at $\varphi = 0.65$. l_f is the curved length of flame root.

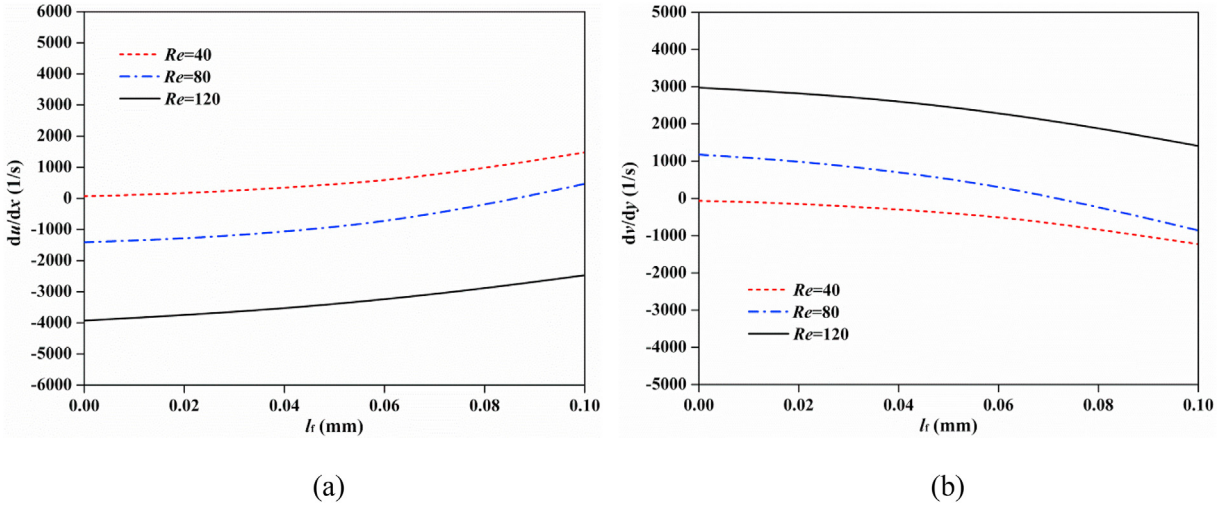

Fig. 11 – The d*u*/d*x* (a) and d*v*/d*y* (b) profiles along with the upstream boundary of flame front from the anchoring location of flame root towards downstream for different *Re* at $\varphi = 0.65$.

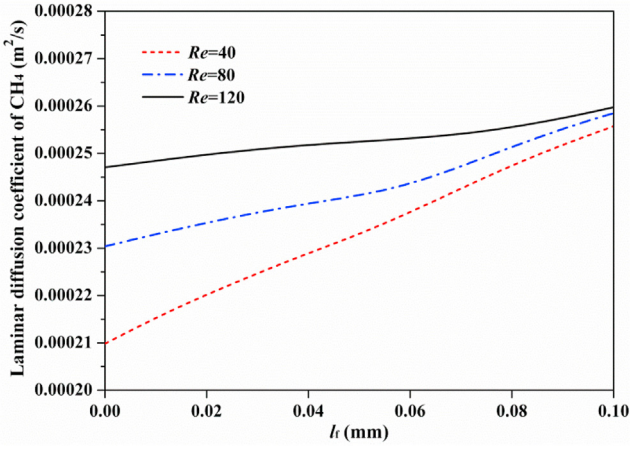

Fig. 12 – The laminar diffusion coefficient profiles of CH_4 along with the upstream boundary of the flame front from the anchoring location of flame root towards downstream for different *Re* at $\varphi = 0.65$.

In order to reveal the reasons for the above distribution characteristics of φ_{local} in Figs. 10 and 11 shows the flow velocity gradient (du/dx and dv/dy) profiles along with the upstream boundary of the flame front towards downstream for different *Re* at $\varphi = 0.65$. It is seen that the |du/dx| and |dv/dy| increases with the increase of *Re*. On the one hand, a larger velocity gradient can enhance the flow two-dimensionality effect, which is beneficial for further improving the preferential transport effect. On the other hand, a larger velocity gradient makes the flammable species in combustion reaction diffuse into the flame root with a faster diffusion velocity. For example, Fig. 12 shows the laminar diffusion coefficient of CH_4 along with the upstream boundary of flame front. The diffusion velocity is faster for a higher *Re*. The above two positive effects result in a larger φ_{local} at the flame root for a higher *Re*.

Critical standoff distance between flame root and holder

Generally, the standoff distance between the flame root and flame holder (l_s) near the blow-off limit increases with the decrease of φ at a constant *Re*, which is confirmed by the present cases of stable flame in Fig. 2. When the flame root is far enough away from the flame holder, the flame will blow off. Therefore, the l_s probably can be used as an index to evaluate the flame stabilization or predict blow-off limit. Here, it is necessary to find the relationship between critical l_s and *Re*. The critical φ is defined as the smallest equivalence ratio below which the flame blows off under a constant *Re*. Accordingly, the l_s for the critical φ is named as the critical l_s. For the bigger *Re* ($\geq$160), the flames are pulsating (*i.e.*, no stable flame behavior) near the blow-off limit (see Fig. 2). However, the pulsating flame at these cases mainly attributes to the pulsation of flame top rather than flame root [35]. The flame root at the pulsating cases in Fig. 2 nearly maintains at the same location, so the average l_s in one cycle of pulsation in the critical case was adopted as the critical l_s. Fig. 13a shows the critical l_s at different *Re*. It can be seen that the critical l_s decreases with *Re*. The relationship between the critical l_s and *Re* presents the function relation of second-order although the relationship between the blow-off limit and *Re* is non-monotonic, which may be the intrinsic relation/unification of the anomalous and normal blow-off. Additional, Fig. 13b presents the function relation between the critical l_s and critical φ for the normal blow-off ($Re \geq 80$). Interestingly, the relationship between the critical l_s and critical φ also presents the function relation of second-order. These two function relations can help us to better predict the critical l_s and blow-off limit at each *Re*. It also helps us to gain insight into the consistency of the anomalous and normal blow-off phenomena.

Conclusions

The present work reports the distribution characteristics of methane/air premixed flame dynamics at different Reynolds numbers in a micro preheated combustor with a flame holder. Interestingly, an anomalous blow-off phenomenon, *i.e.*, the blow-off limit increases with a decreasing *Re*, is observed for the first time. In addition, it is found that the present

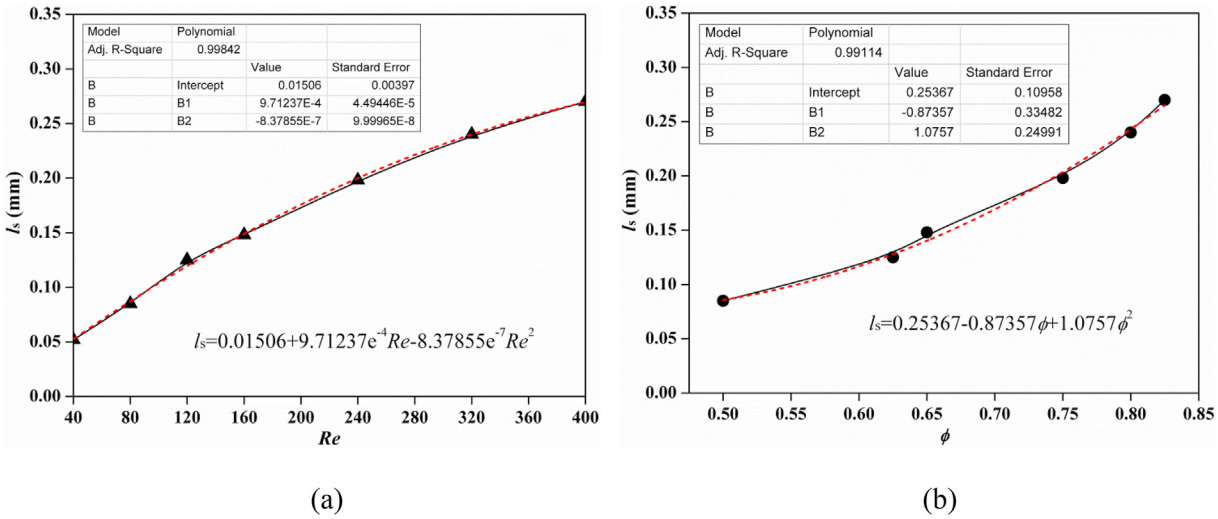

(a) (b)

Fig. 13 – The critical standoff distance between the flame root and flame holder (l_s) for different *Re* (a) and different critical φ (b).

differences of blow-off limit for different *Re* are significantly larger than that in the similar mesoscale combustor, which may be a new feature of flame dynamics in the micro combustor. Then, the underlying mechanisms responsible for the anomalous blow-off are discussed in terms of the flow field, stretch effect, conjugate heat exchange, and preferential transport effect. It is found that the flow field, stretch effect, and the heat loss from the flame root to the flame holder are not the main factors to determine the blow-off limit. A better heat recirculation effect results in the increase of blow-off limit from $Re = 120$ to 80. A worse flow recirculation effect, a larger total heat loss ratio from the combustor to the environment, and a worse preferential transport effect lead to the decrease of blow-off limit from $Re = 80$ to 40. In the end, the relationship between the critical l_s and *Re* is analyzed. It presents the function relation of second-order, which should be the intrinsic unification of the anomalous and normal blow-off. Besides, the relationship between the critical l_s and critical φ in the normal blow-off stage also presents the function relation of second-order.

Declaration of competing interest

The authors declare that they have no known competing financial interests or personal relationships that could have appeared to influence the work reported in this paper.

Acknowledgments

This work was supported by the National Natural Science Foundation of China (No. 51706080) and the Fundamental Research Funds for the Central Universities (2019kfyXJJS110).

REFERENCES

[1] Ju Y, Maruta K. Microscale combustion: technology development and fundamental research. Prog Energy Combust Sci 2011;37:669–715.
[2] Leach TT, Cadou CP. The role of structural heat exchange and heat loss in the design of efficient silicon micro-combustors. Proc Combust Inst 2005;30:2437–44.
[3] Maruta K. Micro and mesoscale combustion. Proc Combust Inst 2011;33:125–50.
[4] Maruta K, Kataoka T, Kim NI, Minaev S, Fursenko R. Characteristics of combustion in a narrow channel with a temperature gradient. Proc Combust Inst 2005;30:2429–36.
[5] Pizza G, Frouzakis CE, Mantzaras J, Tomboulides AG, Boulouchos K. Dynamics of premixed hydrogen/air flames in microchannels. Combust Flame 2008;152:433–50.
[6] Xu B, Ju Y. Experimental study of spinning combustion in a mesoscale divergent channel. Proc Combust Inst 2007;31:3285–92.
[7] Wan JL, Shang C, Zhao H. Dynamics of methane/air premixed flame in a mesoscale diverging combustor with/without a cylindrical flame holder. Fuel 2018;232:659–65.
[8] Kuo CH, Ronney PD. Numerical modeling of non-adiabatic heat-recirculating combustors. Proc Combust Inst 2007;31:3277–84.
[9] Li J, Li Q, Shi J, Liu X, Guo Z. Numerical study on heat recirculation in a porous micro-combustor. Combust Flame 2016;171:152–61.
[10] Liu Y, Fan A, Yao H, Liu W. Numerical investigation of filtration gas combustion in a mesoscale combustor filled with inert fibrous porous medium. Int J Heat Mass Tran 2015;91:18–26.
[11] Li J, Li Q, Wang Y, Guo Z, Liu X. Fundamental flame characteristics of premixed H2–air combustion in a planar porous micro-combustor. Chem Eng J 2016;283:1187–96.
[12] Jiang LQ, Zhao DQ, Wang XH, Yang WB. Development of a self-thermal insulation miniature combustor. Energy Convers Manag 2009;50:1308–13.
[13] Huang W, Yan L. Numerical investigation on the ram–scram transition mechanism in a strut-based dual-mode scramjet combustor. Int J Hydrogen Energy 2016;41:4799–807.
[14] Shanbhogue SJ, Husain S, Lieuwen T. Lean blowoff of bluff body stabilized flames: scaling and dynamics. Prog Energy Combust Sci 2009;35:98–120.
[15] Sun M-b, Zhong Z, Liang J-h, Wang H-b. Experimental investigation on combustion performance of cavity-strut injection of supercritical kerosene in supersonic model combustor. Acta Astronaut 2016;127:112–9.
[16] Wang Z-g, Sun M-b, Wang H-b, Yu J-f, Liang J-h, Zhuang F-c. Mixing-related low frequency oscillation of combustion in an ethylene-fueled supersonic combustor. Proc Combust Inst 2015;35:2137–44.
[17] Yang WM, Chou SK, Shu C, Li ZW, Xue H. Combustion in micro-cylindrical combustors with and without a backward facing step. Appl Therm Eng 2002;22:1777–87.
[18] Ni S, Zhao D, Sun Y, Jiaqiang E. Numerical and entropy studies of hydrogen-fuelled micro-combustors with different geometric shaped ribs. Int J Hydrogen Energy 2019;44:7692–705.
[19] Wan JL, Fan AW, Liu Y, Yao H, Liu W, Gou XL, et al. Experimental investigation and numerical analysis on flame stabilization of CH4/air mixture in a mesoscale channel with wall cavities. Combust Flame 2015;162:1035–45.
[20] Wan JL, Fan AW, Yao H, Liu W. Flame-anchoring mechanisms of a micro cavity-combustor for premixed H2/air flame. Chem Eng J 2015;275:17–26.
[21] Wan JL, Yang W, Fan AW, Liu Y, Yao H, Liu W, et al. A numerical investigation on combustion characteristics of H2/air mixture in a micro-combustor with wall cavities. Int J Hydrogen Energy 2014;39:8138–45.
[22] Wan JL, Fan AW, Yao H, Liu Y, Gou XL, Zhao DQ. The impact of channel gap distance on flame splitting limit of H2/air mixture in microchannels with wall cavities. Int J Hydrogen Energy 2014;29:11308–15.
[23] Wang H, Wang Z, Sun M, Wu H. Combustion modes of hydrogen jet combustion in a cavity-based supersonic combustor. Int J Hydrogen Energy 2013;38:12078–89.
[24] Wan JL, Fan AW, Maruta K, Yao H, Liu W. Experimental and numerical investigation on combustion characteristics of premixed hydrogen/air flame in a micro-combustor with a bluff body. Int J Hydrogen Energy 2012;37:19190–7.
[25] Wan JL, Fan AW, Yao H, Liu W. Experimental investigation and numerical analysis on the blow-off limits of premixed CH4/air flames in a mesoscale bluff-body combustor. At Energ 2016;113:193–203.
[26] Li L, Yang W, Fan A. Effect of the cavity aft ramp angle on combustion efficiency of lean hydrogen/air flames in a micro cavity-combustor. Int J Hydrogen Energy 2019;44:5623–32.
[27] Pan J, Zhang C, Pan Z, Wu D, Zhu Y, Lu Q, et al. Investigation on the effect of bluff body ball on the combustion characteristics for methane/oxygen in micro combustor. At Energ 2020;190:116465.

[28] Pan J, Zhu J, Liu Q, Zhu Y, Tang A, Lu Q. Effect of micro-pin-fin arrays on the heat transfer and combustion characteristics in the micro-combustor. Int J Hydrogen Energy 2017;42:23207–17.
[29] Wan JL, Fan AW. Effect of solid material on the blow-off limit of CH4/air flames in a micro combustor with a plate flame holder and preheating channels. Energy Convers Manag 2015;101:552–60.
[30] Wan JL, Fan AW, Yao H. Effect of the length of a plate flame holder on flame blowout limit in a micro-combustor with preheating channels. Combust Flame 2016;170:53–62.
[31] Wan JL, Xu Z, Zhao H. Methane/air premixed flame topology structure in a mesoscale combustor with a plate flame holder and preheating channels. At Energ 2018;165:802–11.
[32] Wan JL, Zhao H. Effect of thermal condition of solid wall on the stabilization of a preheated and holder-stabilized laminar premixed flame. At Energ 2020;200:117548.
[33] Wan JL, Zhao H. Blowout limit of premixed flame in a micro preheated combustor with a flame holder at different blockage ratios. Int J Hydrogen Energy 2020. https://doi.org/10.1016/j.ijhydene.-2020.06.257.
[34] Wan JL, Cheng X. Numerical investigation of the local extinction and re-ignition mechanisms of premixed flame in a micro combustor with a flame holder and preheating channels. Fuel 2020;264:116837.
[35] Wan JL, Zhao H. Dynamics of premixed CH 4/air flames in a micro combustor with a plate flame holder and preheating channels. At Energ 2017;139:366–79.
[36] Ma Q, Fang R, Xiang L. Handbook of thermo-physical properties. Bejing: China Agricultural Machinery Press; 1986 (in chinese).
[37] Bilger RW, Starner SH. On reduced mechanisms for methane air combustion in nonpremixed flames. Combust Flame 1990;80:135–49.
[38] Kee RJ, Grcar JF, Smooke MD. J.A. Miller. Sandia National Laboratories Report 1994;13. SAND85-8240.
[39] Law CK. Combustion physics. Cambridge: Cambridge University press; 2006.
[40] Fluent 14.0. Canonsburg, PA: User's Guide; 2011.
[41] Wan JL, Zhao H. Thermal performance of solid walls in a mesoscale combustor with a plate flame holder and preheating channels. At Energ 2018;157:448–59.
[42] Wan JL, Zhao H. Blow-off mechanism of a holder-stabilized laminar premixed flame in a preheated mesoscale combustor. Combust Flame 2020;220:358–67.
[43] Shoshin Y, Bastiaans RJM, de Goey LPH. Anomalous blow-off behavior of laminar inverted flames of ultra-lean hydrogen–methane–air mixtures. Combust Flame 2013;160:565–76.
[44] Jiménez C, Michaels D, Ghoniem AF. Ultra-lean hydrogen-enriched oscillating flames behind a heat conducting bluff-body: anomalous and normal blow–off. Proc Combust Inst 2019;37:1843–50.
[45] Wan JL, Zhao H. Experimental study on blow-off limit of a preheated and flame holder-stabilized laminar premixed flame. Chem Eng Sci 2020;223:115754.
[46] Kedia KS, Ghoniem AF. The blow-off mechanism of a bluff-body stabilized laminar premixed flame. Combust Flame 2015;162:1304–15.
[47] Barlow RS, Dunn MJ, Sweeney MS, Hochgreb S. Effects of preferential transport in turbulent bluff-body-stabilized lean premixed CH4/air flames. Combust Flame 2012;159:2563–75.
[48] Kedia KS, Ghoniem AF. The anchoring mechanism of a bluff-body stabilized laminar premixed flame. Combust Flame 2014;161:2327–39.